Published in final edited form as:

Biochemistry. 1988 December 27; 27(26): 9149–9160. doi:10.1021/bi00426a012.

Distance Distributions in Proteins Recovered by Using Frequency-Domain Fluorometry. Applications to Troponin I and Its Complex with Troponin C

Joseph R. Lakowicz[‡], **Ignacy Gryczynski**[‡,§], **Herbert C. Cheung**[‖], **Chien-Kao Wang**[‖], **Michael L. Johnson**[⊥], **Nanda Joshi**[‡]

[‡]University of Maryland at Baltimore.

[§]Permanent address: Institute of Experimental Physics, University of Gdansk, Gdansk, Poland.

[‖]University of Alabama at Birmingham.

[⊥]University of Virginia.

Abstract

We used resonance energy transfer to examine the distribution of distances between two sites on troponin I (TnI). The donor (D) was the single tryptophan residue at site 158 (Trp 158), and the acceptor (A) was cysteine 133 (Cys 133) which was labeled with *N*-(iodoacetyl)-*N*′-(1-sulfo-5-naphthyl)ethylene-diamine (IE). A distribution of D–A distances results in a distribution of donor decay times, which were resolved by using frequency-domain fluorometry. In the native state we recovered a relatively narrow distribution of D–A distances. The widths of the distance distributions were found to increase progressively and dramatically with increasing concentrations of guanidine hydrochloride. Binding of calcium-free troponin C (TnC) to troponin I did not alter the distance distribution. Addition of Ca^{2+} to the TnI·TnC complex resulted in a sharper distance distribution and protected against the guanidine hydrochloride induced increase in the width of the distance distribution. Additionally, the same distance distributions were recovered for native and denatured TnI when the Forster distance for energy transfer was decreased by acrylamide quenching. These results demonstrate that distance distributions can be recovered with good accuracy, to the extent of revealing modest changes due to binding of other components. This technique should have widespread applications in studies of protein folding.

The phenomenon of nonradiative resonance energy transfer has been widely used to measure distance between specific sites in labeled macromolecules (Stryer, 1978; Steinberg, 1971). For any given donor (D)[1]–acceptor (A) pair the extent of energy transfer depends upon the inverse sixth power of the distance $\bar{r}$ between the two sites. The extent of transfer can be used to calculate the distance, as described by Forster (1948). To date, most measurements of energy transfer have been used to estimate specific distances between sites on structured macromolecules. However, there are many circumstances where a single distance is not expected to exist. For instance, consider a protein that can exist in a native or a denatured

[1]Abbreviations: A, acceptor; D, donor; DTT, dithiothreitol; EGTA, ethylene glycol bis(β-aminoethyl ether)-*N*,*N*,*N*′,*N*′-tetraacetic acid; Gdn-HCl, guanidine hydrochloride; hw, half-width, full width of the Gaussian at the half-maximum intensity; IE, *N*-(iodoacetyl)-*N*′-(1-sulfo-5-naphthyl)ethylenediamine; IE-TnC, IE-labeled TnC; TnC, troponin C; TnI, troponin I.

state (Scheme I). In the native state the ensemble of protein molecules is expected to display a relatively sharp D–A distance distribution, whose average value is determined by specific features of the folded structure. In contrast, the random coil molecules will exist in a range of conformations, and the ensemble is expected to show a wide range of D–A distances.

Our objective is to recover the D–A distance distribution $P(r)$. It is generally not possible to obtain such distribution by using only the steady-state data, unless one uses a number of D–A pairs that are each characterized by different values for the Forster distance (Cantor & Pechukas, 1971) or unless the Forster distance is varied by collisional quenching (Gryczynski et al., 1988a,b). The former requires many differently labeled proteins, which is too difficult to accomplish on a routine basis. In contrast, it is possible to obtain information on $P(r)$ for a single D–A pair from the time-dependent decays of the donor fluorescence. This is because each D–A distance results in a different decay time for the donor. Hence, a dispersion of D–A distances results in a dispersion of decay times. Such measurements have been successfully performed by Haas and co-workers using time-correlated photon counting (Grinvald et al., 1972; Haas et al., 1975; Amir & Haas, 1987).

The basic difficulty in recovering D–A distances is obtaining adequate resolution of the intensity decays. In previous years the resolution was limited by the relatively low repetition rate of the flash lamp sources and by the low intensity of the lamp pulses. These factors result in excessively long data acquisition times for adequate statistical accuracy in the data. Additionally, the measurements were limited to relatively long lifetimes because of the 1–2-ns pulse widths of the flash lamps (O'Connor & Phillips, 1985). This situation has now changed because of the introduction of laser sources with picosecond pulse widths and megahertz repetition rates (Visser & Wampler, 1985), but these sources have not yet been used to recover distance distributions. Alternatively, it is now possible to recover complex decays in the frequency domain by using instrumentation recently developed in two laboratories (Gratton & Limkeman, 1983; Lakowicz & Maliwal, 1985; Lakowicz et al., 1986a).

In the present report we used the frequency-domain measurements to recover distance distributions in troponin I. This protein is one of three subunits of troponin, which is involved in the calcium regulation of skeletal and cardiac muscle. Troponin I provides an excellent system for distance distribution studies because it contains a single tryptophan residue at position 158 which serves as the donor. TnI can be specifically labeled with IE on cysteine 133 (Wang & Cheung, 1986), which provides a single acceptor. Additionally, TnI is known to bind troponin C and to be stabilized by binding to calcium-saturated TnC (Cheung et al., 1987). Our measurements indicate that denaturation of TnI results in a dramatic increase in the D–A distance distribution and that these distributions are sensitive to TnC in the presence of calcium.

Theory

The theory for energy transfer in the presence of a range of D–A distances is relatively unfamiliar and will thus be presented in detail. The effect of a distance distribution is most easily revealed by assuming the decay of the donor, in the absence of acceptor, is a single

exponential. Hence, this simpler theory is presented first, followed by the slightly more complex expressions for a multiexponential decay of the donor.

Single-Exponential Donor Decay.

Assume the decay of the donor [$I_D(t)$], in the absence of energy transfer, is a single exponential

$$I_D(t) = I_D^0 \exp(-t / \tau_D) \tag{1}$$

where τ_D is the decay time of the donor. If a single acceptor is present at a unique distance r, then donor decay is given by

$$I_{DA}(r,t) = I_D^0 \exp(-t / \tau_D - k_{DA}t) \tag{2}$$

The rate of energy transfer is given by

$$k_{DA} = (1 / \tau_D)(R_0 / r)^6 \tag{3}$$

with R_0 being the Forster distance. The decay of the donor remains a single exponential in the presence of a single acceptor at a distance r. The single-exponential decay time is

$$1 / \tau_{DA} = 1 / \tau_D + k_{DA} \tag{4}$$

The widespread use of energy transfer for distance measurements is partially a result of the simple decay predicted for a single D–A distance. The efficiency of energy transfer is given by

$$E = 1 - \tau_{DA} / \tau_D \tag{5}$$

and can be used to calculate the D–A distance according to

$$E = R_0^6 / (R_0^6 + r^6) \tag{6}$$

The Forster distance R_0 can be calculated from the spectral properties of the chromophores:

$$R_0^6 = \frac{9000(\ln 10)\kappa^2 \phi_D}{128\pi^5 N n^4} \int_0^\infty F_D(\lambda)\, \epsilon_A(\lambda)\, \lambda^4\, d\lambda \tag{7}$$

where κ^2 is the orientation factor, ϕ_D is the quantum yield of the donor in the absence of the acceptor, n is the refractive index, N is Avogadro's number, $F_D(\lambda)$ are the emission spectra of the donor with the area normalized to unity, $\epsilon_A(\lambda)$ is the absorption spectrum of the acceptor in units of M^{-1} cm^{-1}, and λ is the wavelength in nanometers. The calculated distances are somewhat uncertain to an extent dependent upon the extent of static and dynamic averaging of the orientation factor (Dale et al., 1979; Dale & Eisinger, 1975). In

our analysis we assume the value of κ^2 is equal to $^2/_3$ due to the range of conformations, the possibility of rotational diffusion, and the mixed polarization of the species (Haas et al., 1978). It should be noted that the use of $\kappa^2 = {}^2/_3$ is not likely to result in significant error if the donor and acceptor can adopt a range of conformations (Englert & Leclerc, 1978).

The intensity decay of the donor becomes more complex if the acceptor is located over a range of D–A distances. Suppose that the D–A pair is connected via a random coil peptide chain and the solution is too dilute for transfer between nonbonded D–A pairs. Since each individual D–A pair is characterized by some specific distance r, the intensity decay of each donor is still a single exponential and is given by

$$I(r,t) = k \exp\left[-\frac{t}{\tau_D} - \frac{t}{\tau_D}\left(\frac{R_0}{r}\right)^6\right] \tag{8}$$

However, the observed decay contains contributions from D–A pairs at all possible distances and is thus more complex than a single exponential. The intensity decay of the donor is given by the average of the individual decays weighted by the distance probability distribution [$P(r)$] of the D–A pairs (Haas et al., 1975):

$$I_{DA}(t) = I_D \int_0^\infty P(r) \exp\left[-\frac{t}{\tau_D} - \frac{t}{\tau_D}\left(\frac{R_0}{r}\right)^6\right] dr \tag{9}$$

This expression is appropriate for a distribution that is static during the lifetime of the donor. In our case the decay time of the donor is 3 ns or less. In aqueous solution at 5 °C a small molecule such as indole will have a diffusion constant near 0.4×10^5 cm^2/s. During 3 ns such a molecule may diffuse a distance [$(\Delta\chi^2)^{1/2} = (2Dt)^{1/2}$] of 15 Å. Hence, our assumption of a static D–A distribution may not be completely correct. However, the donor and acceptors are covalently linked to peptide chains, so that the actual diffusion coefficients will be smaller than predicted for indole itself. Additionally, the presence of diffusion will probably result in more averaging of the D–A distribution and less dispersion in the intensity decay. Hence, if diffusion has any effect on the recovered D–A distributions, it is likely to result in apparent widths that are somewhat smaller than the instantaneous average.

In this report we assume that the probability distribution is a Gaussian:

$$P(r) = \frac{r^n}{\sigma\sqrt{2\pi}} \exp\left[-\frac{1}{2}\left(\frac{r-\bar{r}}{\sigma}\right)^2\right] \tag{10}$$

where $\bar{r}$ is the average, σ is the standard deviation of the distribution, and $n = 0$, 1, or 2. The standard deviation is related to the half-width hw, (full width at half-maximum) by hw = 2.354σ. The use of a Gaussian is clearly an approximation, which may be refined by further experimentation. The choice of the exponent for r depends upon whether one assumes the D–A distance distribution is a Gaussian along a line, in a plane, or in three dimensions. For an infinite flexible chain all possible solid angles are available at each distance, and the appropriate factor is r^2 (Flory, 1969). However, the selection of n is less obvious for a

structured protein, for which the acceptor may be restricted to a limited range of solid angles. Importantly, we recovered visually similar distance distributions irrespective of the choice of $n = 0$, 1, or 2.

Frequency-Domain Expressions.

We recovered the intensity decay of the donor or the D–A pair from the frequency response of its emission. In the frequency domain one measures the phase (ϕ_ω) and modulation (m_ω) of the emission over a range of modulation frequencies (ω). It should be remembered that even if the donor decays as a single exponential (eq 1), the decay of the D–A pair will be nonexponential if there exists a range of D–A distances (eq 9). We generally analyze the data for both donor and the donor–acceptor using the multiexponential model:

$$I(t) = \sum_i \alpha_i \exp(-t/\tau_i) \tag{11}$$

where α_i are the preexponential factors and τ_i the associated decay times. A range of D–A distances is expected to increase the complexity of the decay and thus require more components to fit the data. For eq 11 or for any intensity decay law, the frequency response (ϕ_ω and m_ω) can be calculated by using

$$N_\omega = \frac{\int_0^\infty I(t) \sin \omega t \, dt}{\int_0^\infty I(t) \, dt} \tag{12}$$

$$D_\omega = \frac{\int_0^\infty I(t) \cos \omega t \, dt}{\int_0^\infty I(t) \, dt} \tag{13}$$

For the multiexponential decay law these transforms can be represented analytically (Lakowicz et al., 1984) by

$$N_\omega = \frac{1}{J} \sum_i \frac{\alpha_i \omega \tau_i^2}{1 + \omega^2 \tau_i^2} \tag{14}$$

$$D_\omega = \frac{1}{J} \sum_i \frac{\alpha_i \tau_i}{1 + \omega^2 \tau_i^2} \tag{15}$$

where the normalization factor is given by $J = \sum_i \alpha_i \tau_i$. For a distribution of D–A distances and a single-exponential decay of the donor in the absence of acceptor, the transforms are calculated numerically. Since both $I(t)$ and $P(r)$ are continuous and well-behaved functions with continuous derivatives, the order of integration can be reversed, yielding

$$N_\omega = \frac{1}{J}\int_{r=0}^{\infty} \frac{P(t)\omega\tau_{DA}{}^2}{1+\omega^2\tau_{DA}{}^2}\,dr \tag{16}$$

$$D_\omega = \frac{1}{J}\int_{r=0}^{\infty} \frac{P(r)\tau_{DA}}{1+\omega^2\tau_{DA}{}^2}\,dt \tag{17}$$

where the normalization factor J is given by

$$J = \left[\int_0^\infty P(r)\,dr\right]\left[\int_0^\infty I_{DA}(t)\,dt\right] \tag{18}$$

Depending upon $P(r)$, the integral from $r = 0$ to infinity may not be equal to unity. This integral will be less than unity when part of the distribution occurs below $r = 0$. The use of $\int_0^\infty P(r)$ in eq 18 is equivalent to normalizing this integral to unity. It should be remembered that eq 16 and 17 contain τ_{DA}, which is itself dependent upon the D–A distance (eq 4). Hence, one sees the similarities between the expressions for a multiexponential decay and for a distance distribution. In each instance N_ω and D_ω are weighted averages that depend on $P(r)$ and the decay times.

The parameters describing the intensity decay (α_i and τ_i or $\bar{r}$ and $\bar{\sigma}$) are found by using nonlinear least squares (Bevington, 1969). The calculated (c) phase and modulation values for the assumed decay law are given by

$$\phi_{c\omega} = \arctan\left(N_\omega / D_\omega\right) \tag{19}$$

$$m_{c\omega} = \left(N_\omega{}^2 + D_\omega{}^2\right)^{1/2} \tag{20}$$

The parameter values are estimated by minimizing $\chi_R{}^2$:

$$\chi_R{}^2 = \frac{1}{\nu}\sum_\omega \left(\frac{\phi_\omega - \phi_{c\omega}}{\delta\phi}\right)^2 + \frac{1}{\nu}\sum_\omega \left(\frac{m_\omega - m_{c\omega}}{\delta m}\right)^2 \tag{21}$$

where ν is the number of degrees of freedom and $\delta\phi$ and δm are the experimental uncertainties in the measured phase and modulation values.

Estimation of the uncertainties in the recovered parameters is a difficult problem. We used three different methods, each of which resulted in similar estimated uncertainties. Our analysis programs calculate the uncertainties by examination of the range of parameter values that are consistent with the data (Johnson, 1983). We also examined the dependence of $\chi_R{}^2$ surfaces for fixed values of the parameters following adjustment of the other values to minimize $\chi_R{}^2$. Both these methods should account for correlation between the

parameters, which allows the parameter values to vary in a concerted manner without significantly altering χ_R^2. And finally, we used repetitive simulations and analyses of data with random noise added at a level comparable to the experimental uncertainties.

Multiexponential Donor Decays.

The intensity decays of most proteins, even those containing a single tryptophan residue, are usually multiexponential (Beechem & Brand, 1985; Grinvald & Steinberg, 1976; Lakowicz et al., 1986b). More specifically, we found that the intensity decay of the donor in TnI (Trp 158) could not be described by a single decay time. Hence, it was necessary to use somewhat more complex expressions which account for a multiexponential decay law in the absence of energy transfer. We believe this is an important generalization, as previous measurements have been restricted to donors that display single-exponential intensity decays (Amir & Haas, 1986; Amir et al., 1986; Haas et al., 1975, McWerther et al., 1986).

We fit the decays of the donor alone using a sum of exponentials

$$I_D(t) = \sum_i \alpha_{Di} \exp(-t / \tau_{Di}) \tag{22}$$

where α_{Di} are the preexponential factors and τ_{Di} the associated decay times for the donor in the absence of any acceptor. We assumed that the Forster distances for transfer from each component in the donor decay are the same. Hence, the transfer rates are given by

$$k_{DAi} = (1 / \tau_{Di})(R_0 / r)^6 \tag{23}$$

and the distance-dependent donor decay times are given by

$$1 / \tau_{DAi} = 1 / \tau_{Di} + (1 / \tau_{Di})(R_0 / r)^6 \tag{24}$$

We do not have experimental data to rigorously defend this assumption, but we can argue that it is reasonable. Different Forster distances would be expected for each component if the emission spectra of each component were distinct. However, the intensity decays of proteins are only weakly dependent upon emission wavelength, especially in the central region of the emission which was used for our measurements (Lakowicz & Cherek, 1980; Demchenko, 1986). Under this assumption the intensity decay of a D–A pair spaced by a distance r is given by

$$I_{DA}(r,t) = \sum_i \alpha_{Di} \exp\left[-t / \tau_{Di} - \frac{t}{\tau_{Di}}\left(\frac{R_0}{r}\right)^6\right] \tag{25}$$

and the observed decay is given by

$$I_{DA}(t) = \int_0^\infty P(r)\, I_{DA}(r,t)\, dr \tag{26}$$

The sine and cosine transforms are

$$N_\omega = \int_0^\infty \sum_i \frac{P(r)\alpha_{Di}\omega\tau_{DAi}^2}{1+\omega^2\tau_{DAi}^2}\,dr \tag{27}$$

$$D_\omega = \int_0^\infty \sum_i \frac{P(r)\alpha_{Di}\tau_{DAi}}{1+\omega^2\tau_{DAi}^2}\,dr \tag{28}$$

It is important to notice that a multiexponential decay for the donor does not introduce any additional parameters into the analysis. This is because the intrinsic decays of the donor are measured in a separate experiment, using samples without acceptor. The data from the donor are fit to the multiexponential model, and the parameters (α_{Di}, and τ_{Di}) are held constant in eq 27 and 28 during the least-squares analysis. It should be remembered that τ_{DAi} depends on distance (eq 24).

It is probable that the tryptophan intensity decays of TnI are more complex than a multiexponential. The decay could be the result of a distribution of decay times (James & Ware, 1986; Alcala et al., 1987a,b; Lakowicz et al., 1987c) or due to transient effects in intrinsic quenching processes (Lakowicz et al., 1987b,d). While the triple-exponential model may not be completely correct, this will not affect the recovered distribution of distances. The only requirement is that the form and parameters used to represent the donor decay provide an accurate representation of this decay. This is accomplished by the three-exponential model, which provides good fits to the data.

Variation of the Forster Distance by Collisional Quenching.

The ability to recover a distance distribution is always dependent upon the value of R_0, which defines a range of distances over which the transfer is significantly dependent upon distance. When the D–A distance is less than $0.46R_0$ or greater than $2.15R_0$, then transfer is either 99% or 1% efficient, respectively (eq 6), and the data are unlikely to be sensitive to the values of $P(r)$ outside this range. We expanded the detectable range of distances using collisional quenching of the donor by acrylamide. Collisional quenching decreases the quantum yield of the donor and thereby decreases R_0 (eq 7). Elsewhere we demonstrated that the appropriate quantum yields are given by the dynamic or collisional component in the quenching (Gryczynski et al., 1988a,b). Hence, the appropriate quantum yields are given by

$$\phi_D^Q = \phi_D^0 / (1 + k_D[Q]) \tag{29}$$

where ϕ_D^0 is the quantum yield in the absence of quenching, k_D is the dynamic quenching constant, and [Q] is the concentration of quencher (Lakowicz, 1983). The quenching-dependent Forster distances are then given by

$$R_0^Q = R_0(\phi_D^Q / \phi_D^0)^{1/6} \tag{30}$$

Data measured at a single value of R_0^Q can be analyzed by using eq 21-28 with the appropriate value of R_0^Q. These analyses reveal whether $P(r)$ depends upon the distance window. Alternatively, the data at several R_0^Q values (quencher concentrations) may be analyzed simultaneously (globally) to recover a single distance distribution. In this case the sum in eq 21 extends over both the frequencies (ω) and the quencher concentrations [Q]. Since quenching widens the distance window, the distance distributions recovered from the global analysis should be more reliable than the individually recovered distributions.

Materials and Methods

Frequency-domain measurements were performed on the instrument described previously in detail (Lakowicz et al., 1986a). The excitation source was a 3.79-MHz train of pulses, about 7 ps wide, obtained from the cavity-dumped output of a synchronously pumped rhodamine 6G dye laser. The dye laser output was frequency-doubled to 295 nm. This source is intrinsically modulated to many gigahertz and is used to directly excite the sample. For excitation of IE we used a second pyridine II dye laser, frequency-doubled to 360 nm. The modulated emission was detected by using a microchannel plate photomultiplier tube, R1564U (Hamamatsu Corp.), which was externally cross-correlated. All intensity decays were measured by using rotation-free polarization conditions, with the donor emission selected by a 340-nm interference filter, 10-nm bandwidth. Where necessary, the emission from the acceptor was selected with a 500-nm interference filter. For all analyses and simulations the uncertainties in the phase ($\delta\phi$) and modulation (δm) values were taken as 0.2° and 0.005, respectively. For the simulations we used data for about 22 frequencies, spaced approximately equally in a logarithmic scale from 10 to 320 MHz.

Anisotropy decays were obtained from the frequency response of the polarized emission (Lakowicz et al., 1985; Maliwal & Lakowicz, 1986). The data were fit to a double-exponential anisotropy decay law

$$r(t) = \sum_i r_i \exp(-t / \theta_i) \tag{31}$$

where r_i are the amplitudes of the components associated with the correlation times θ_i.

TnI and TnC were isolated as described previously. Briefly, troponin was obtained from rabbit skeletal muscle as described by Cheung et al. (1982). TnC was isolated from troponin as described by Perry and Cole (1974). Troponin B (TnI·TnC complex) was isolated as described by Wilkinson (1974) and was used as the starting material for isolation of TnI and TnC. The isolated subunits were shown to be homogeneous by SDS/polyacrylamide gel electrophoresis. Protein concentrations were determined by using $E(1\%) = 2.3$ at 277 nm for TnC (Murray & Kay, 1972) and $E(1\%) = 3.97$ at 280 nm for TnI (Wilkinson, 1974). The molecular weights of TnC and TnI were taken as 18000 and 21000, respectively.

TnI was labeled on Cys 133 with IE as described previously (Wang & Cheung, 1986). TnI was labeled as the TnI·TnC complex, as this protects the other two cysteine residues from modification. In all cases the extent of modification was higher than 98%. The proteins were dissolved in 0.4 M KCl, 50 mM Tris, and 1 mM EGTA, with 0.5 mM DTT, pH 7.5, for all

experiments except those involving Gdn-HCl. In this case 5 M Gdn-HCl replaced the 0.4 M KCl. All experiments were performed at 5 °C with TnI concentrations near 35 μM. Mg^{2+} or Ca^{2+} was added to yield concentrations near 2 mM. Forster distances were obtained from Wang (1979), and these values were calculated by using corrected emission spectra for TnI.

Results

Simulated Data for Distance Distributions.

Prior to the presentation of experimental results it seems informative to demonstrate the effects of a distance distribution on the frequency response of the donor. This is best accomplished with simulated data. Analysis of simulated data, with appropriate levels of random noise, reveals the resolution possible from the measurements. Alternatively stated, the expected uncertainties in the values of $\bar{r}$ and hw can be predicted from least-squares analysis of simulated data with random noise. We now know from several years experience that our experimental uncertainties are consistently near $\delta\phi = 0.2°$ and $\delta m = 0.005$ and that these random errors appear to determine the available resolution. Hence, simulated data with this level of random error should provide an accurate prediction of the resolution possible from the experimental data.

For the simulations we chose parameter values that are comparable to those found for TnI. Hence, R_0 was assumed to be 20 Å, the average distance ($\bar{r}$) was 25 Å, τ_D was 3 ns, and the hw was varied from 0.1 to 50 Å. These assumed values result in about 25% transfer, which is comparable to that found for transfer from Trp 158 to the IE-labeled Cys 133.

Figure 1 shows simulated data for the donor alone with an assumed single-exponential decay time of 3 ns (○), and for the D–A pair separated by a single distance of 25 Å, hw = 0.5 Å (●). The solid lines represent the best single-exponential fits to the data. The effect of the acceptor is to decrease the decay time by about 25% from 3 to 2.3 ns. This decrease in decay time is the origin of the shift of the frequency response to higher frequencies in the presence of acceptor (Figure 1). The location of the acceptor at a single distance from the donor does not introduce any heterogeneity into the frequency response. This is seen by the small and random deviations from the single-exponential model.

If the D–A pair is not characterized by a single distance, then the decay of the donor becomes more heterogeneous. This is seen from attempts to fit the data simulated for a half-width of 50 Å to a single-exponential model (Figure 2). For this broad distribution (50 Å) the frequency response shows increased dispersion, and the data cannot be fit by the single-exponential model. For this particular data set the value of χ_R^2 is 52.7 for the single-exponential fit. This value is easily adequate to reject the single decay time fit, as values of χ_R^2 that are 1.1-fold larger than the minimum are expected to occur with a probability of less than 33% for random errors and our degrees of freedom ($\nu = 46$). As the hw is decreased, the donor decays are expected to become more like a single exponential. The lower limit for visually obvious deviations (lower panels) appears to be about 10 Å for the hw. However, even for hw = 10 Å the values of χ_R^2 for the single-exponential fit are near 12. Hence, it appears that the frequency-domain measurements are easily capable of detecting the existence of a distribution of distances.

The simulation in Figure 2 demonstrates that a half-width of 50 Å is easily detected by deviations from the single-exponential model. We then questioned the accuracy with which we could recover $\bar{r}$ and hw from our data. This was accomplished by repetitive simulations with different sets of random noise, followed by least-squares analysis. This method provides realistic estimates of the uncertainties, and if incorrect, these are overestimates (Lakowicz et al., unpublished observations). The results of these analyses are summarized in Table I. The hw was increased progressively from 0.1 to 50 Å. Irrespective of the hw the analysis returned correct values of $\bar{r}$ and hw (Table I). The standard deviations (SD) of the recovered values of $\bar{r}$ and hw are quite small, typically less than 0.4 Å except for the largest half-widths. In these cases the uncertainty in the hw is as large as 6 Å, which is still only 10% of the 50-Å hw. This is probably the result of displacement of the acceptor into regions of complete transfer or no transfer. Hence, the upper and lower limits are not accurately available from the data.

Table I also contains the range of parameter values consistent with the data, calculated with consideration of correlation between the parameters (Johnson, 1983). The range of $\bar{r}$ values is rather small, typically ±0.2 Å or less. The range of the half-widths is always ±2 Å or greater. While these uncertainties are larger than those recovered from the multiple analyses, the values are still modest. Hence, the simulations indicate that we can recover values of $\bar{r}$ and hw to within ±2 Å or less, which is adequate for our purposes. It is interesting to notice that the range of half-widths consistent with the data is asymmetric for the large half-widths. For $\bar{r}$ = 25 Å the range extends further toward longer distances. This is probably due to displacement of the acceptor beyond the range of significant transfer. The opposite is found if $\bar{r} < R_0$. In this case ($\bar{r}$ = 15 Å, hw = 50 Å) the uncertainty interval extends a greater distance toward shorter distances. This is because the transfer becomes essentially complete, and the closely spaced D–A pairs do not contribute to the measured donor decay.

We questioned the minimum hw detectable by our measurements. This was accomplished by simulating the frequency response with increasing half-widths, followed by analysis of the data with a single-exponential model (Table I). As the simulated width is increased above 5 Å, χ_R^2 increases rapidly. A significant 1.34-fold elevation of χ_R^2 was found for a 5-Å half-width. These results suggest we could measure the half-widths of distributions as narrow as 5 Å, should such narrow distributions exist in TnI.

And finally, we questioned the ability of our algorithm to recover the distance distributions when the intensity decay is multiexponential. For this purpose we simulated data with τ_{Di} values of 0.3, 1.0, and 3.0 ns, with all the α_{Di} = 0.333. The heterogeneity of the donor decay did not prevent recovery of $\bar{r}$ or hw (Table I) and did not increase the uncertainties in these values. The value of χ_R^2 for the single decay time fits is always large due to the heterogeneity of the donor decay. As the width of the distribution is increased, the value of χ_R^2 increases further. For instance, the value of χ_R^2 increases from 445 to 638 as the hw is increased from 1 to 50 Å. A similar effect was seen in our experimental data for the D–A pairs.

An alternative representation of the uncertainties in the hw can be obtained by examining the values of χ_R^2 as the hw is held fixed at a range of incorrect values (Figure 3). While the half-widths were held constant, the value of $\bar{r}$ was varied to yield the minimum value of χ_R^2. The range of $\bar{r}$ and hw consistent with the data is approximately given by the range of values for which χ_R^2 is elevated to an extent possible 67% of the time due to random errors. The χ_R^2 surfaces were found to be sensitive to the half-width, with greater sensitivity for smaller half-widths (Figure 3). This analysis predicts uncertainties that are comparable to those summarized in Table I. For a hw = 5 Å the uncertainty is ±1.5 Å, and for hw = 50 Å the uncertainty is ±3 Å. We believe this is the worst case analysis, which provides upper limits to the uncertainties. Nonetheless, the simulations indicate that our experimental data are adequate to recover distributions of the type found for TnI.

Emission Spectra and Donor Decays of TnI.

Emission spectra of TnI and IE-labeled TnI are shown in Figure 4. The emission from the IE acceptor occurs near 480 nm and does not overlap with the tryptophan donor emission at 360 nm. The tryptophan emission of TnI was similar for all the conditions described in this report. This emission shifts little in the presence of TnC and/or Ca^{2+} and does not shift significantly in the presence of 6 M Gdn-HCl. This insensitivity to conditions, and the relatively long wavelength emission maximum, suggests that Trp 158 is mostly exposed to the aqueous phase. The location of this residue near the surface of the protein is also suggested by the anisotropy decay, which is described below in greater detail. Both the steady-state anisotropies and the time-dependent anisotropies suggest considerable motional freedom of Trp 158.

We determined the intensity decays of Trp 158 in TnI under a variety of conditions, which include the absence (D) and presence (D + A) of acceptor, and both D and D + A in the presence of TnC, Ca^{2+}, Mg^{2+} or 6 M Gdn-HCl. The multiexponential fits to the frequency responses are summarized in Table II. Representative data are shown in Figure 5. In every case the presence of the IE acceptor results in an approximate 20% decrease in the apparent single-exponential decay time and a shift in the frequency response to higher frequencies (Figure 5). In contrast to the simulated data where the donor decay was assumed to be a single exponential, the decay of Trp 158 is heterogeneous irrespective of the presence or absence of acceptor. Consequently, it is difficult to see any acceptor-induced heterogeneity in the frequency responses (Figure 5). However, the value of χ_R^2 from the single decay time fits do indicate increased heterogeneity due to the acceptor. Examination of Table II reveals that χ_R^2 for the single decay time fits increases by about 100 for each D–A pair, relative to the donor alone. This effect is similar to that found for the simulated data for a multiexponential donor (Table I). It is this increase in heterogeneity that is used to determine the distance distribution between the D and A sites.

Distribution of D–A Distances in TnI.

The frequency-domain intensity decays of TnI were used to calculate the distance distributions, characterized by $\bar{r}$ and hw for an assumed Gaussian (eq 10). The most dramatic effect was observed upon comparison of TnI in the native state and denatured by 5 M Gdn-HCl (Figure 6, top). In the native state the width of the distribution is relatively narrow (hw

= 11.5 Å), and this width increases to 56 Å upon denaturation. The average distance we recovered for TnI (24 Å) is in good agreement with the value of 22 Å observed previously (Wang & Cheung, 1985). Importantly, the form of the distribution is mostly independent of the model used for its estimation. For the narrow distributions the parameter values do not depend strongly on the value of *n*. This is illustrated in Table III for TnI, where the values of $\bar{r}$ and hw are similar, irrespective of *n*. Similar results were found for all samples not containing Gdn-HCl. For the wide distribution, with 5 M Gdn-HCl, the parameter values depend strongly on *n* (Table III). Nonetheless, the distributions are visually similar, irrespective of the value of *n*. This is illustrated in the upper panel of Figure 6, which shows the distributions recovered with different volume elements for the integration (*n* = 0, 1, or 2 in eq 10). Irrespective of the choice of *n* the D–A distances are seen to be widely distributed from 10 to 50 Å. We note that this is the worst case. For all the other samples, with sharper distributions, the differences between *n* = 0, 1, and 2 are visually insignificant.

Under our experimental conditions TnI and TnC bind stoichiometrically, yielding a TnI·TnC complex. We examined the effect of complex formation on the D–A distribution in TnI (Figure 6, bottom). Perhaps surprisingly, binding of TnC results in an increase in the width of the distribution from 11.5 to 19.7 Å (Table III). TnC is known to bind Ca^{2+}, and addition of Ca^{2+} to the complex results in a decrease in the width from 19.7 to 11.5 Å. We note that the experiments were performed in duplicate, with completely new samples, and the results were in excellent agreement with those summarized in Tables II and III. In the second experiment a Ca^{2+}-dependent decrease in the half-width was also observed, but the width was 14.5 Å instead of 11.5 Å.

The simulations have already indicated that we can recover half-widths of 10 Å with little uncertainty. Nonetheless, we questioned whether the half-widths summarized in Table III were in fact determined by the data, or whether the measurements lacked resolution, resulting in the relatively wide half-widths. Hence, we fit the data to narrow distributions with hw = 2 Å and allowed $\bar{r}$ to vary to minimize χ_R^2 (Table III). In each case χ_R^2 was elevated severalfold, indicating that the data are not consistent with a narrow D–A distribution. The increase in χ_R^2 with a fixed hw of 2 Å is smallest for the complex with TnC and Ca^{2+} because the hw is small.

We examined the range of half-widths consistent with our data by examination of the χ_R^2 surfaces (Figure 7). These surfaces were calculated by holding the hw fixed at the values indicated on the *x* axis and allowing $\bar{r}$ to vary so as to minimize χ_R^2. For native TnI there is little uncertainty in the half-width, with the range being from 10.5 to 12.5 Å. For denatured TnI the range is larger, from 40 to 67 Å. However, the surfaces do not overlap on the hw axis with any reasonable value for χ_R^2, which indicates that the D–A distribution for the denatured state is significantly different from that of the native state. Surprisingly, the same may be said for the half-width of the TnI·TnC complex, with and without Ca^{2+} (Figure 7, lower panel). Once again, the surfaces do not intersect below the 67% cutoff, which indicates the half-widths are significantly different in the absence and presence of Ca^{2+}.

Progressive Denaturation of TnI.

Our ability to resolve subtle differences in the D–A distributions of TnI resulted in an attempt to detect a progressive increase in the half-widths upon denaturation by Gdn-HCl. The results are summarized in Figure 8. The hw for TnI increases progressively from 12 to 50 Å as the concentration of Gdn-HCl is increased from 0 to 5 M. Additionally, the average distance ($\bar{r}$) increases in a similar manner. The midpoint of the transition is near 1.5 M Gdn-HCl, which is in agreement with other studies on TnI (Cheung, unpublished data). TnI is known to be stabilized against denaturation by complexation with TnC + Ca^{2+}. This protection is evident in Figure 8, which shows little change in $\bar{r}$ or hw for the complex at Gdn-HCl concentrations ranging to 3.5 M.

Effect of the Forster Distance on Distance Distributions.

And Finally, we used collisional quenching by acrylamide to decrease the Forster distances. These data are shown in Figure 9 for native and denatured TnI, and the values of R_0^Q are summarized in Table IV (Gryczynski et al., 1988a). In the presence of acrylamide the frequency response of IE-TnI shifts to higher frequencies. The solid lines indicate the best fit to all the data using a single distribution. This indicates the data are consistent with the distribution found in the absence of quenching. This point is further illustrated in Figure 10, which shows the values of $\bar{r}$ and hw recovered from global analysis using four R_0^Q values (---) and from analysis of each file for each R_0^Q value. The recovered distance distributions do not depend significantly on the Forster distance, at least over the limited range accessible by collisional quenching.

Anisotropy Decays of the Donors and Acceptors.

It is known that calculated distances can be in error due to the orientation factor κ^2 (Dale et al., 1979; Dale & Eisinger, 1975). To estimate the possible effects of κ^2 on our analyses, we measured both the steady-state and time-resolved anisotropies of the donor and acceptor. Typical frequency-domain anisotropy data are shown in Figure 11. For both native and denatured TnI the frequency distribution of the differential phase angles is non-Lorentzian, which indicates the presence of more than a single rotational correlation time. For a molecule with a rotational correlation time near 10 ns, and no internal flexibility, one expects the maximum differential phase angle to be near 40 MHz. However, the phase angles increase with modulation frequency to about 200 MHz, suggesting the presence of subnanosecond components in the anisotropy decays. Least-squares analyses of these data indicate that nearly 50% of the total anisotropy decays with correlation times near 0.7 ns. These components are somewhat longer (1.2–1.4 ns) in the TnI·TnC complexes, but in all cases the tryptophan residue displays substantial segmental freedom in excess of overall rotational diffusion (Table V). Similarly, the anisotropy decay of the acceptor also displays both fast and slow components. These data and the steady-state anisotropies (Table VI) are used under Discussion estimate the possible effects of κ^2 on the widths of the distance distributions.

Discussion

In the previous sections we demonstrated that distance distributions between two sites on troponin I could be recovered from the donor decays, measured in the frequency domain. It now seems appropriate to describe the meaning of the derived distances and half-widths. In the case of denatured TnI a wide range of distances was expected and observed. In the case of native TnI the widths ranged from 11 to 20 Å, which appears to be rather wide for a native protein. There are two possible origins of these widths, these being the effects of κ^2 on the transfer rates and the possibility that the donor and/or acceptor have motional freedom. In fact, the emission spectra and anisotropy decays of Trp 158 indicate this residue is mobile and mostly exposed to the aqueous phase. Similarly, the emission spectra and anisotropy decays of the acceptor indicate this residue is also mobile. On the basis of the bond lengths and number of bonds it seems probable that the Trp 158 and IE-Cys 133 could migrate about 5 Å, respectively, on the surface of the protein. Hence, the combined displacements of these residues could easily contribute 10 Å in width to the distance distribution.

Alternatively, the width may be due to the effects of κ^2. The effects of κ^2 on the measured distances and distance distributions have been the subject of considerable controversy (Dale et al., 1979; Dale & Eisinger, 1974, 1976; Haas et al., 1978). The formalism developed by Dale et al. (1979) probably represents the maximum uncertainty in the distance due to the unknown value of κ^2. This theory assumes the absorption and emission are due to single transition moments. According to Dale et al. (1979), the maximum and minimum values of κ^2 can be calculated from the depolarization of the donor and acceptor which is due to segmental motion of these residues:

$$\kappa_{\min}{}^2 = {}^2/_3\,[1 - (d_{\mathrm{D}}{}^x + \mathrm{d}_{\mathrm{A}}{}^x)\,/\,2] \tag{32}$$

$$\kappa_{\max}{}^2 = {}^2/_3\,(1 + d_{\mathrm{D}}{}^x + d_{\mathrm{A}}{}^x + 3d_{\mathrm{D}}{}^x d_{\mathrm{A}}{}^x) \tag{33}$$

where

$$d_i{}^x = (r_i\,/\,r_0)^{1\,/\,2} \tag{34}$$

The value of r_i should represent the fractional depolarization due to segmental motion of the residue (d_i), but not the depolarization due to overall rotational diffusion of the protein (d_{P}). These values are related to the steady-state anisotropy (r) by

$$r = r_0 d_l d_{\mathrm{P}} \tag{35}$$

where

$$d_{\mathrm{P}}{}^{-1} = 1 + \tau\theta_{\mathrm{P}} \tag{36}$$

and τ is the decay time of the probe and θ_P the rotational correlation time of the protein (Lakowicz & Weber, 1980). Since the theory of Dale et al. (1979) assumes single transition moments it may be appropriate to use $r_0 = 0.4$ for both the donor and the acceptor. However, we chose the more conservative approach of using the values of r_0 appropriate for each probe (Trp or IE) in the absence of rotational diffusion. These assumptions result in the depolarization factors for segmental motions summarized in Table VI. The average values $\langle d_D{}^x \rangle$ and $\langle d_A{}^x \rangle$ are 0.745 and 0.683, respectively, which yields a lower limit of $\kappa_{min}{}^2 = 0.19$ and an upper limit of $\kappa_{max}{}^2 = 2.64$. These values of κ^2 indicate that the distances can range from 0.81 to 1.26 of the apparent distance ($\bar{r}$). For instance, for the average distance of 24 Å found for TnI, the maximum range is 19.5–30 Å, which would be a half-width near 10 Å. This half-width is comparable to the values recovered for TnI but smaller than that found for denatured TnI. Hence, it appears that the effects of orientation can add about 10 Å to the apparent widths.

The range of orientation factors can also be estimated from the time-resolved anisotropy decays. If the data are adequate to recover the amplitudes of both the local motion and overall rotational diffusion, then

$$d_i = (r_i / r_0)^{1/2} \tag{37}$$

where r_0 is the total anisotropy and i indicates either donor or acceptor. The value of r_i is the amplitude of the anisotropy decay which is due to overall rotation diffusion (Dale & Eisinger, 1974) and is associated with the long correlation time. Using the values in Table V, we recovered d_i values ranging from 0.44 to 0.79, with an average value for the donor and the acceptor of 0.64 and 0.68, respectively. This yields upper and lower limits of κ^2 of 0.23 and 2.42. These κ^2 values in turn imply a range of distances from 0.84 to 1.25 of the distance found for $\kappa^2 = ⅔$. For our average distances near 24 Å, the range is thus 20–30 Å, or a width of about 10 Å, which is in agreement with the results from the steady-state anisotropy data.

It should be noted that the analyses described above are the worst case predictions of the effects of κ^2. We did not include the effects of depolarization during energy transfer, which would result in a smaller possible range of κ^2 values. Additionally, the anisotropies of both Trp and IE indicate the transitions are mixed. According to Haas et al. (1978) this results in a smaller possible range of distances due to orientation effects. Using Table III of this reference and r_0 values of 0.25 for Trp and IE, one obtains a range of distances from 0.91 to 1.11 of the apparent values. For the example described above ($\bar{r}$ = 24 Å) the range is 21.8–26.6, for a width of 5 Å. This estimate probably reflects the effects of κ^2 on the width of the distribution, whereas the previous calculations based on Dale et al. (1979) probably represent the extreme values of the distance consistent with the data. And finally, we note that the widest distribution of D–A distances was found for denatured TnI. If the D–A distributions we recovered were due predominantly to orientation effects, then one effects a narrow distribution for denatured TnI because the donors and acceptors are more mobile. On the basis of these considerations, we believe the apparent widths found for native TnI are too large to be explained by the effects of the orientation factor.

It should also be emphasized that we recovered the distance distributions using the intrinsic tryptophan emission of TnI. Previous measurements of distance distributions used donors with long decay times and/or single-exponential decays (Haas et al., 1975; Amir & Haas, 1987; Amir et al., 1986). We were able to overcome both restrictions. First, we were able to use the intrinsic emission of tryptophan, with a decay time near 3 ns. This was possible because the frequency-domain measurements provide good resolution of multiexponential decays, even when the mean decay times are less than 1 ns. This capability is illustrated by the substantial decrease in χ_R^2 observed for the double and triple decay time fits (Table I), and elsewhere from studies of highly quenched samples (Lakowicz et al., 1987b) and intrinsic tyrosine fluorescence from proteins (Lakowicz et al., 1987a). Second, our theory and algorithm does not require that the donor decay be a single exponential. This requires an assumption regarding the individual transfer rates but in return provides a more general approach to measuring distance distributions.

It seems appropriate to describe other situations where resolution of distance distributions can be useful. First, it should be emphasized that the method described herein is one of the few methods by which we can recover a conformational distribution. Most physical methods, such as light scattering, NMR, and gel filtration, yield only average dimensions for the macromolecule. Measurement of conformational distributions should have wide-ranging applications in biochemistry. The most obvious application is the measurement of end-to-end distributions for labeled peptides. Such data can be compared with the distribution predicted from the rotation potential functions (Cantor & Schimmel, 1980) or with Monte Carlo calculations on peptides (Premilat & Herman, 1973; Premilat & Margret, 1979) and can thereby serve to test the validity of the potential functions. Additionally, it may be possible to follow the detailed steps in protein folding and thereby gain insight into the stepwise or continuous nature of this process. Additional applications include measurements of lipid distributions in membranes or ion distributions around polyelectrolytes.

Acknowledgments

J.R.L. thanks the National Science Foundation for support of the frequency-domain method and Henry Chong for assistance with the simulations.

Registry No. Trp, 73-22-3; Cys, 52-90-4; Ca, 7440-70-2.

This work was supported by Grants GM-35154 (J.R.L.) and AR-25193 (H.C.C.) from the National Institutes of Health, with support for instrumentation from the National Science Foundation (DMB-8511065 and DMB-8502835). This work was supported in part by the Medical Biotechnology Center, University of Maryland.

References

Alcala JR, Gratton E, & Prendergast FG (1987a) Biophys. J 51, 587–596. [PubMed: 3580485]

Alcala JR, Gratton E, & Prendergast FG (1987b) Biophys. J 51, 597–604. [PubMed: 3580486]

Amir D, & Haas E (1987) Biochemistry 26, 2162–2175. [PubMed: 2441742]

Amir D, Levy DP, & Levin Y (1986) Biopolymers 25, 1645–1658. [PubMed: 2429713]

Beechem JM, & Brand L (1985) Annu. Rev. Biochem 54, 43–71. [PubMed: 3896124]

Bevington PR (1969) Data Reduction and Error Analysis for the Physical Sciences, McGraw-Hill, New York.

Cantor CR, & Pechukas P (1971) Proc. Natl. Acad. Sci. U.S.A 68, 2099–2101. [PubMed: 16591942]

Cantor CR, & Schimmel PR (1980) Biophysical Chemistry, Part I, pp 253–309, W. H. Freeman, New York.

Cheung HC, Wang C-K, & Garland F (1982) Biochemistry 21, 5135–5142. [PubMed: 7171543]

Cheung HC, Wang C-K, & Malik NA (1987) Biochemistry 26, 5904–5907. [PubMed: 3676297]

Dale RE, & Eisinger J (1974) Biopolymers 13, 1573–1605.

Dale RE, & Eisinger J (1975) in Biochemical Fluorescence Concepts (Chen RF, & Edelhoch H, Eds.) Chapter 4, pp 115–284, Marcel Dekker, New York.

Dale RE, & Eisinger J (1976) Proc. Natl. Acad. Sci. U.S.A 73, 271–273. [PubMed: 1061130]

Dale RE, Eisinger J, & Blumberg WE (1979) Biophys. J 26, 161–194. [PubMed: 262414]

Demchenko AP (1986) Ultraviolet Spectroscopy of Proteins, pp 154–158, Springer-Verlag, Berlin.

Englert A, & Leclerc M (1978) Proc. Natl. Acad. Sci. U.S.A 75, 1050–1051. [PubMed: 16592504]

Flory PJ (1969) Statistical Mechanics of Chain Molecules, Wiley-Interscience, New York.

Forster Th. (1948) Ann. Phys. (Leipzig) 2, 55–75 (translated by Knox RS, University of Rochester).

Gratton E, & Limkeman M (1983) Biophys. J 44, 315–324. [PubMed: 6661490]

Grinvald A, & Steinberg IZ (1976) Biochim. Biophys. Acta 427, 663–678. [PubMed: 5134]

Grinvald A, Haas E, & Steinberg IZ (1972) Proc. Natl. Acad. Sci. U.S.A 69, 2273–2277. [PubMed: 16592008]

Gryczynski I, Wiczk W, Johnson ML, & Lakowicz JR (1988a) Chem. Phys. Lett 145, 439–446.

Gryczynski I, Wiczk W, Johnson ML, Cheung HC, Wang CK, & Lakowicz JR (1988b) Biophys. J (submitted for publication).

Haas E, Wilchek M, Katchalski-Katzir E, & Steinberg IZ (1975) Proc. Natl. Acad. Sci. U.S.A 72, 1807–1811. [PubMed: 1057171]

Haas E, Katchalski-Katzir E, & Steinberg IZ (1978) Biochemistry 17, 5064–5070. [PubMed: 718874]

Johnson ML (1983) Biophys. J 44, 101–106. [PubMed: 6626675]

Lakowicz JR (1983) Principles of Fluorescence Spectroscopy, Chapter 9, pp 257–301, Plenum, New York.

Lakowicz JR, & Cherek H (1980) J. Biol. Chem 255, 831–834. [PubMed: 7356662]

Lakowicz JR & Weber G (1980) Biophys. J 32, 591–601. [PubMed: 7248463]

Lakowicz JR, & Maliwal BP (1985) Biophys. Chem 21, 61–78. [PubMed: 3971026]

Lakowicz JR, Laczko G, Cherek H, Gratton E, & Limkeman M (1984) Biophys. J 46, 463–477. [PubMed: 6498264]

Lakowicz JR, Cherek H, Maliwal BP, & Gratton E (1985) Biochemistry 24, 376–383. [PubMed: 3978080]

Lakowicz JR, Laczko G, & Gryczynski I (1986a) Rev. Sci. Instrum 57, 2499–2506.

Lakowicz JR, Laczko G, Gryczynski I, & Cherek H (1986b) J. Biol. Chem 261, 2240–2245. [PubMed: 3944133]

Lakowicz JR, Laczko G, & Gryczynski I (1987a) Biochemistry 26, 82–90. [PubMed: 3828310]

Lakowicz JR, Johnson ML, Gryczynski I, Joshi N, & Laczko G (1987b) J. Phys. Chem 91, 3277–3285.

Lakowicz JR, Cherek H, Gryczynski I, Joshi N, & Johnson ML (1987c) Biophys. Chem 28, 35–50. [PubMed: 3689869]

Lakowicz JR, Joshi NB, Johnson MJ, Szmacinski H, & Gryczynski I (1987d) J. Biol. Chem 262, 10907–10910. [PubMed: 3611095]

Maliwal BP, & Lakowicz JR (1986) Biochim. Biophys. Acta 873, 161–172. [PubMed: 3756173]

McWerther CA, Haas E, Lied AR, & Scheraga HA (1986) Biochemistry 25, 1951–1963. [PubMed: 3707922]

Murray AC, & Kay CM (1972) Biochemistry 11, 2622–2627. [PubMed: 5045520]

O'Connor DV, & Phillips D (1985) Time-Correlated Single Photon Counting, Academic, New York.

Perry SV, & Cole HA (1974) Biochem. J 141, 733–743. [PubMed: 4377105]

Premilat S, & Herman J Jr. (1973) J. Chem. Phys 59, 2602–2612.

Premilat S, & Margret B (1979) J. Chem. Phys 66, 3418–3425.

Steinberg IZ (1971) Annu. Rev. Biochem 40, 83–114. [PubMed: 4331120]
Stryer L (1978) Annu. Rev. Biochem 47, 819–846. [PubMed: 354506]
Visser AJWG, & Wampler JR (1985) Anal. Instrum. (N.Y.) 14, 193–566.
Wang C-K (1985) Ph.D. Thesis, University of Alabama at Birmingham.
Wang C-K, & Cheung HC (1986) J. Mol. Biol 191, 509–521. [PubMed: 2950237]
Wilkinson JM (1974) Biochim. Biophys. Acta 359, 379–388. [PubMed: 4855003]

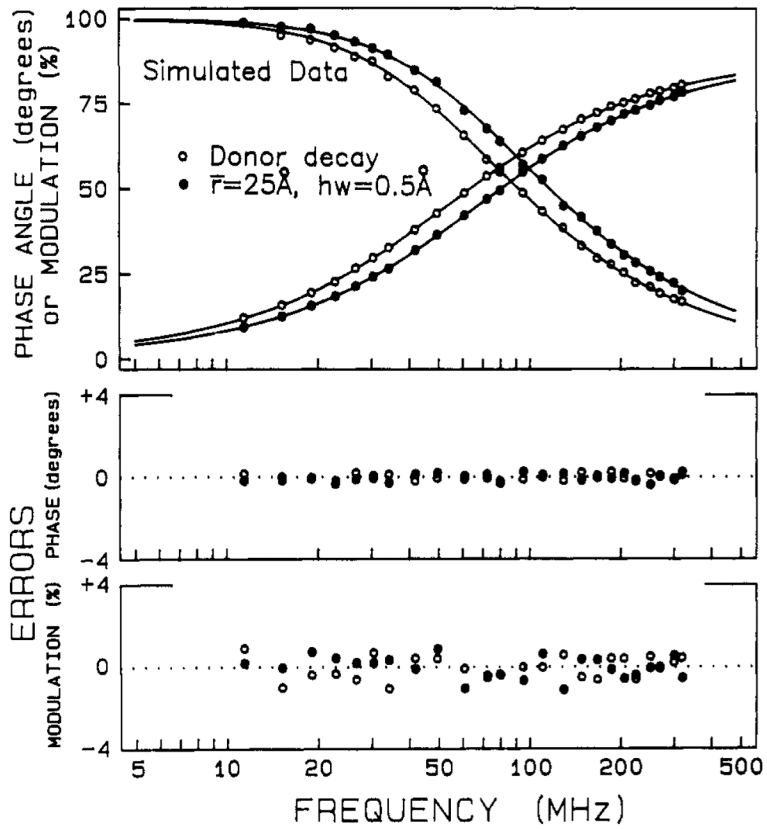

Scheme I:

Illustration of a D–A Pair at a Single Distance (Left) and a Range of D–A Distances (Right)

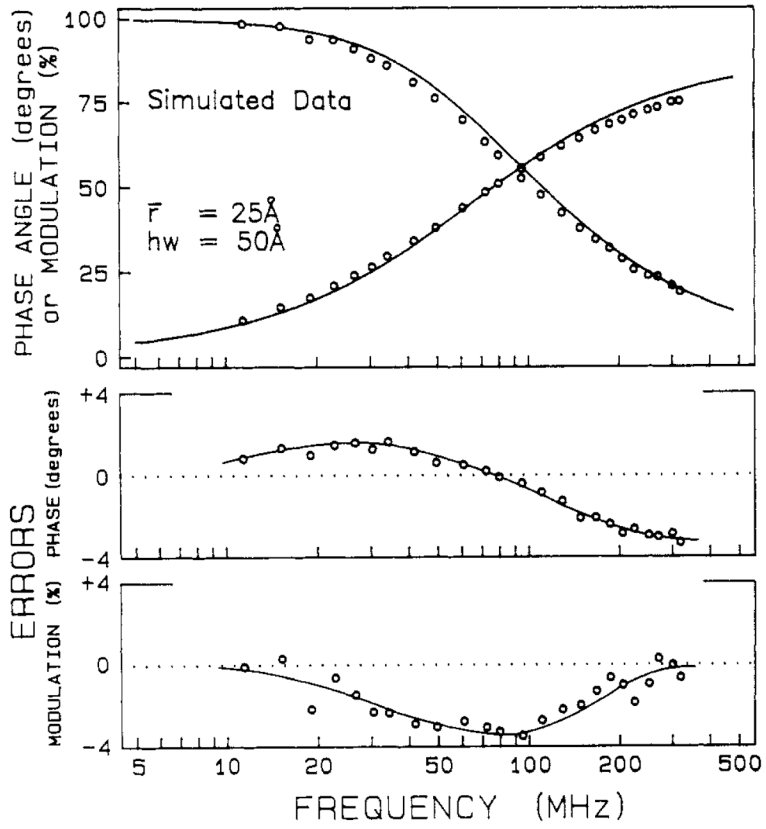

FIGURE 1:

Simulated frequency-domain data for a donor (τ_D = 3 ns, ○) and for a D–A pair (●) with R_0 = 20 Å, $\bar{r}$ = 25 Å, and hw = 0.5 Å. The dots show the simulated values and the solid lines the best single-exponential fits to the data. The lower panels show the deviations between the data and the best single decay time fits. The values of χ_R^2 for a single decay time fit are 0.93 (○) and 0.98 (●) for the donor and D–A pair, respectively.

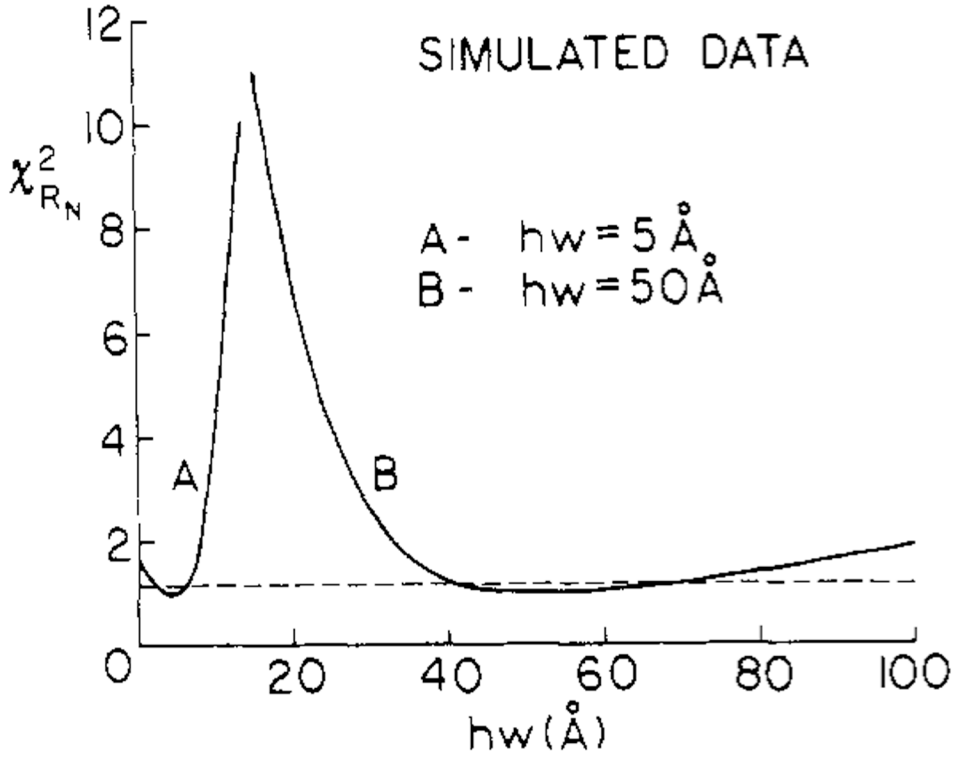

FIGURE 2:

Simulated frequency response data for a D–A pair with hw = 50 Å, R_0 = 20 Å, $\bar{r}$ = 25 Å, and τ_D = 3 ns. The solid lines show the best single exponential fit and the lower panels the deviations from this model, χ_R^2 = 52.7.

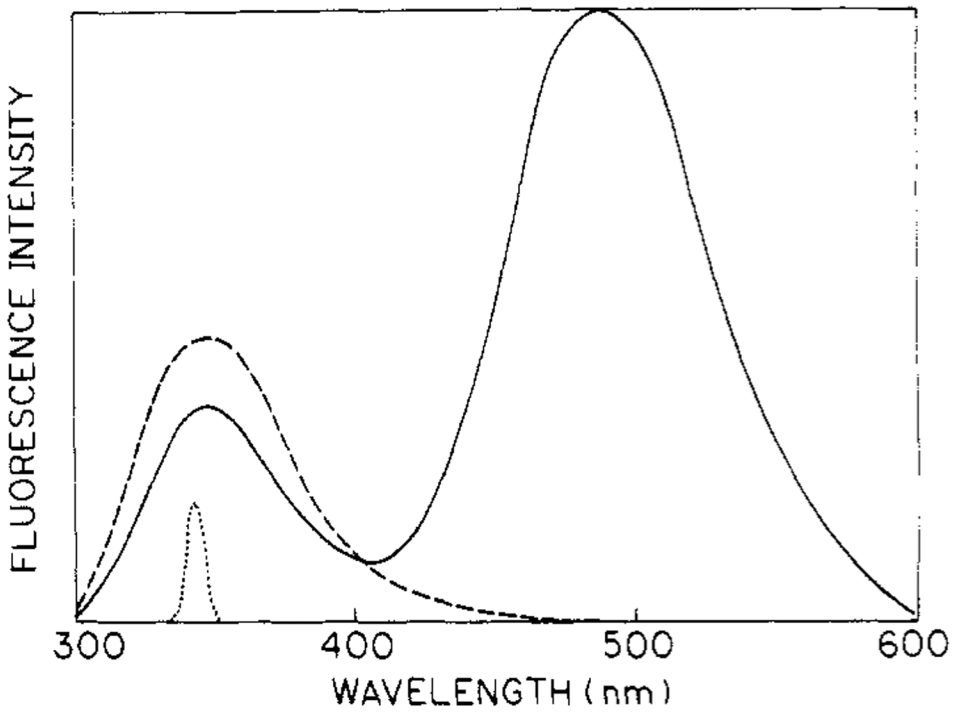

FIGURE 3:

χ_R^2 surfaces for simulated frequency-domain data with τ_D = 3 ns, R_0 = 20 Å, $\bar{r}$ = 25 Å, and hw = 5 (A) or 50 Å (B). The dashed line shows the upper value of χ_R^2 consistent with the χ_R^2 value being due to random errors in 67% of multiple measurements.

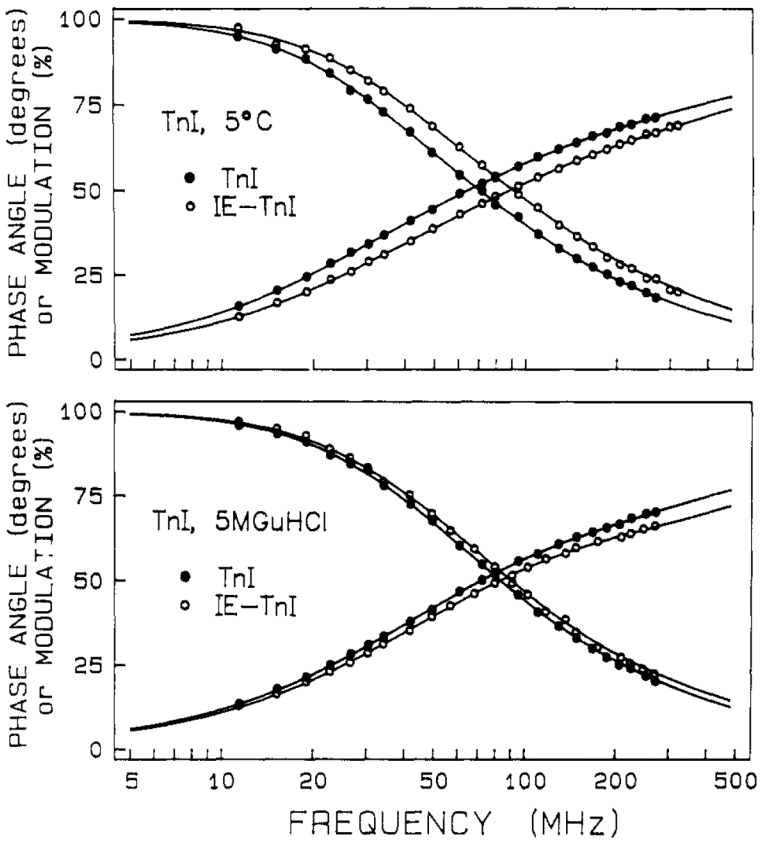

FIGURE 4:

Emission spectra of TnI. Spectra shown for TnI with (—) and without (---) the IE acceptor on Cys 133. The spectral intensities are adjusted to reflect the values for the same concentration of TnI. Also shown is the emission spectrum recorded through the 340-nm interference filter which was used to isolate the donor emission for the intensity decay measurements (···). The excitation wavelength 295 nm; 0.4 M KCl, 50 mM Tris, 1 mM EGTA, and 0.5 mM DTT, pH 7.5, 5 °C.

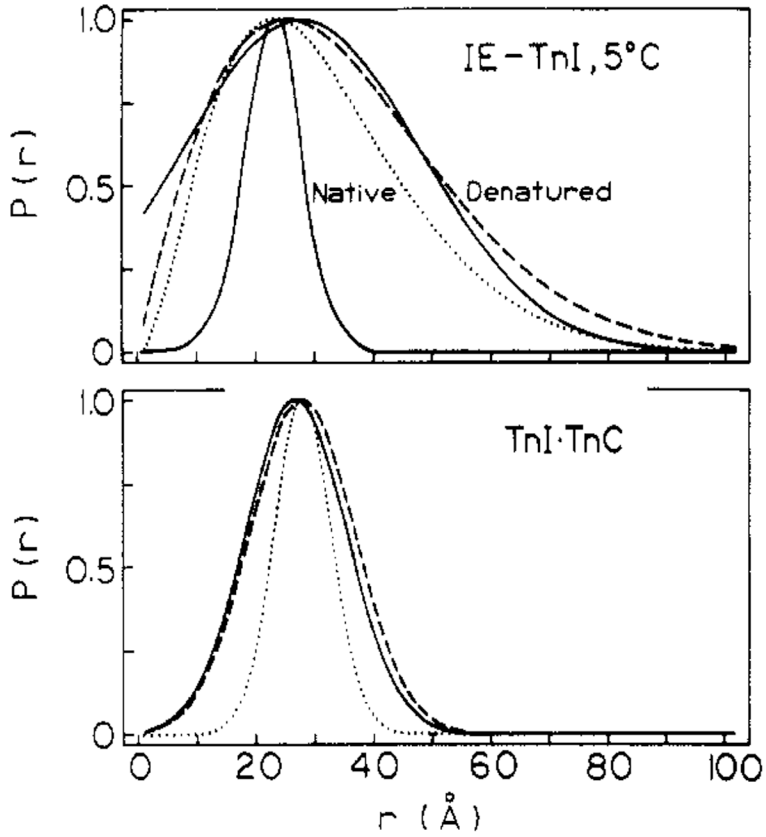

FIGURE 5:

Frequency responses of TnI (●) and IE-TnC (○) in the absence (top) and presence (bottom) of 5 M Gdn-HCl. In each case the solid lines represent the best fits to the data using three decay times (Table II).

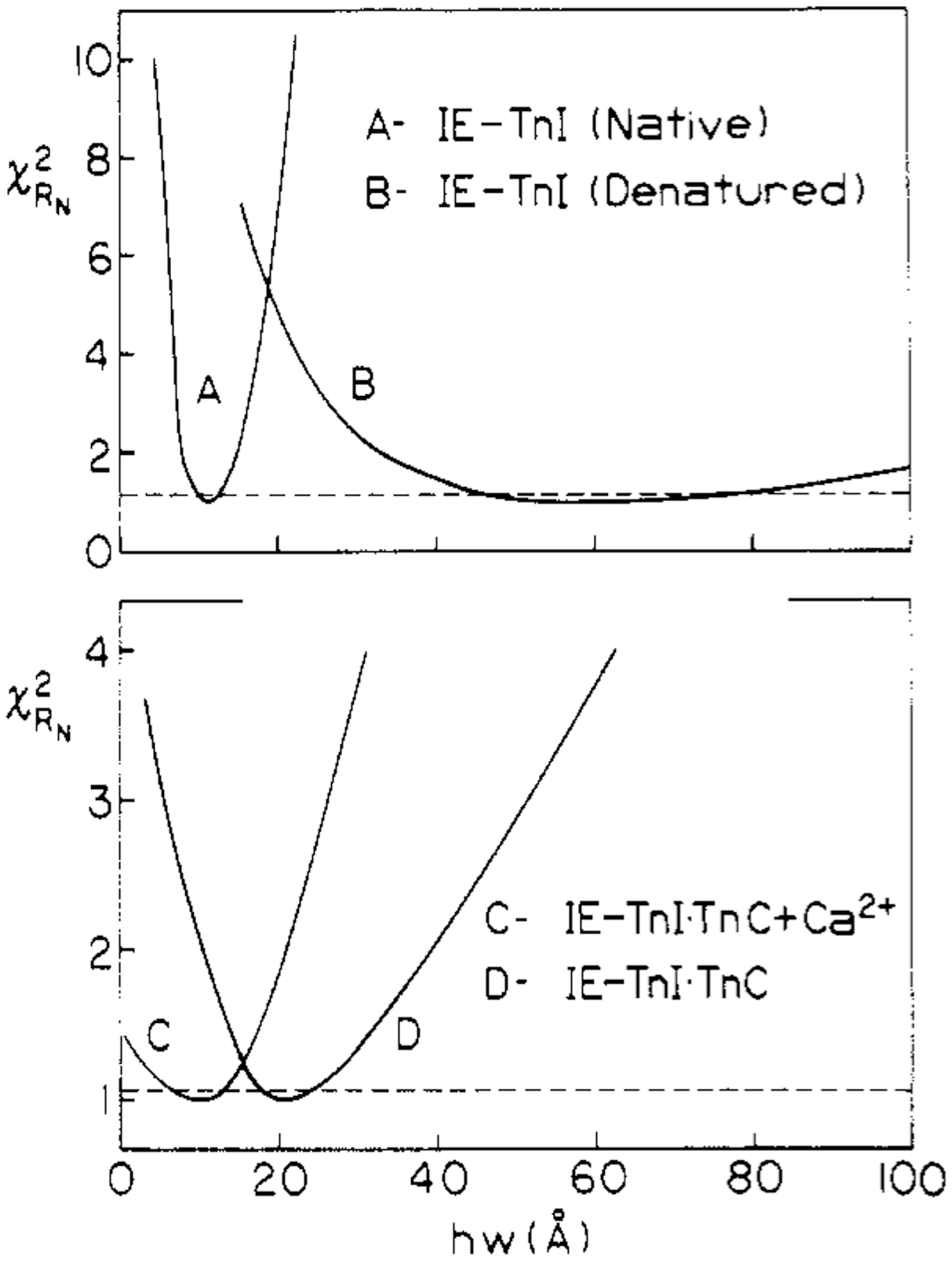

FIGURE 6:

Distance distributions for TnI, TnI·TnC complexes, and denatured TnI. The upper panel shows a comparison of native and denatured TnI (—), recovered with $n = 0$ in eq 10. Also shown are the distributions recovered with $n = 1$ (---) and $n = 2$ (···) for the denatured state. The lower panel shows the distributions for the TnI·TnC complex in the presence of EGTA (—), Mg^{2+} (---), or Ca^{2+} (···). The $P(r)$ curves are peak normalized to facilitate visual comparison.

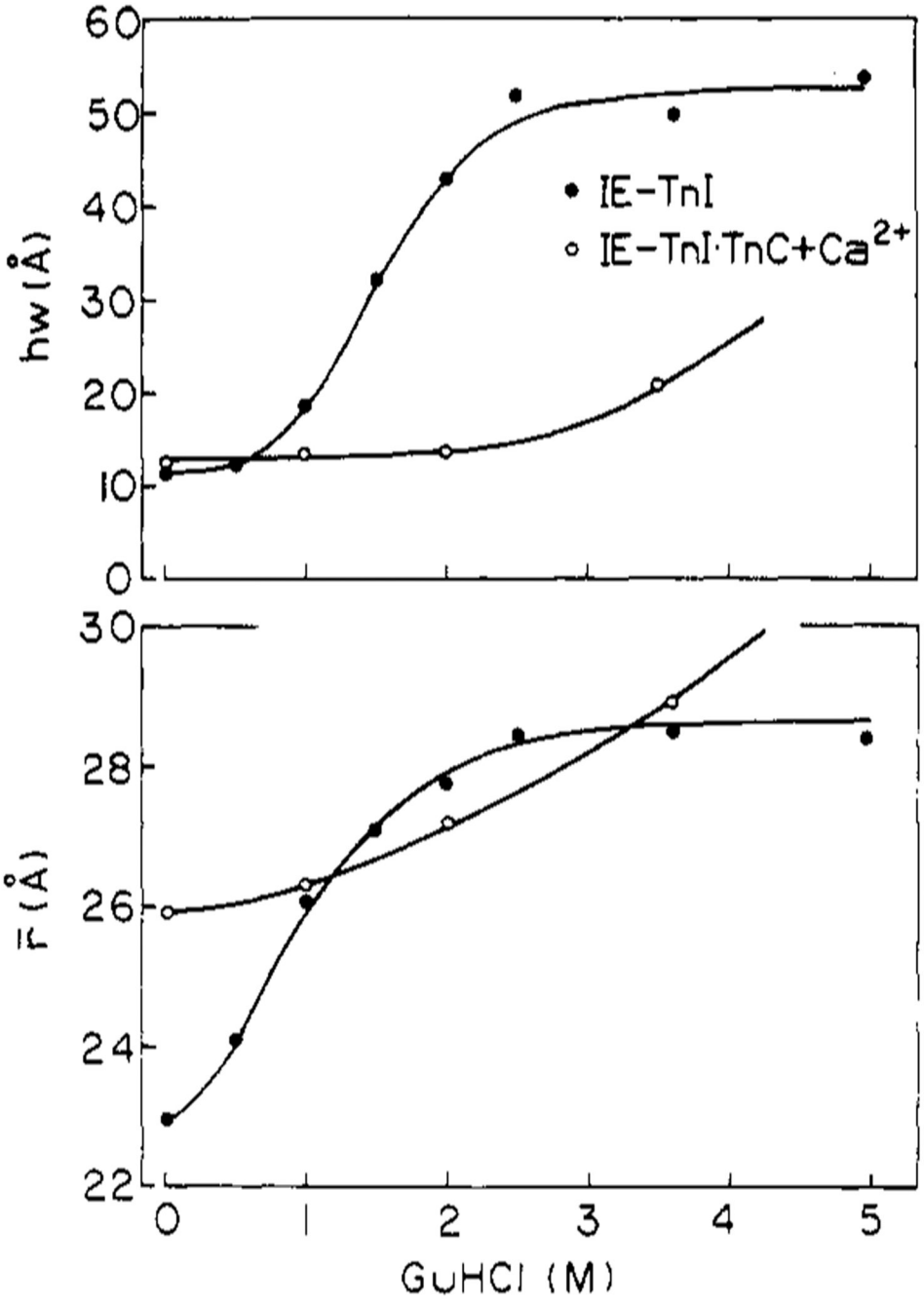

FIGURE 7:

Dependence of χ_R^2 on the half-widths of the D–A distributions in troponin I. Top: Native and denatured TnI. Bottom: TnI·TnC with and without Ca^{2+}. The dashed lines indicate the highest values of χ_R^2 with random noise in 67% of repetitive measurements.

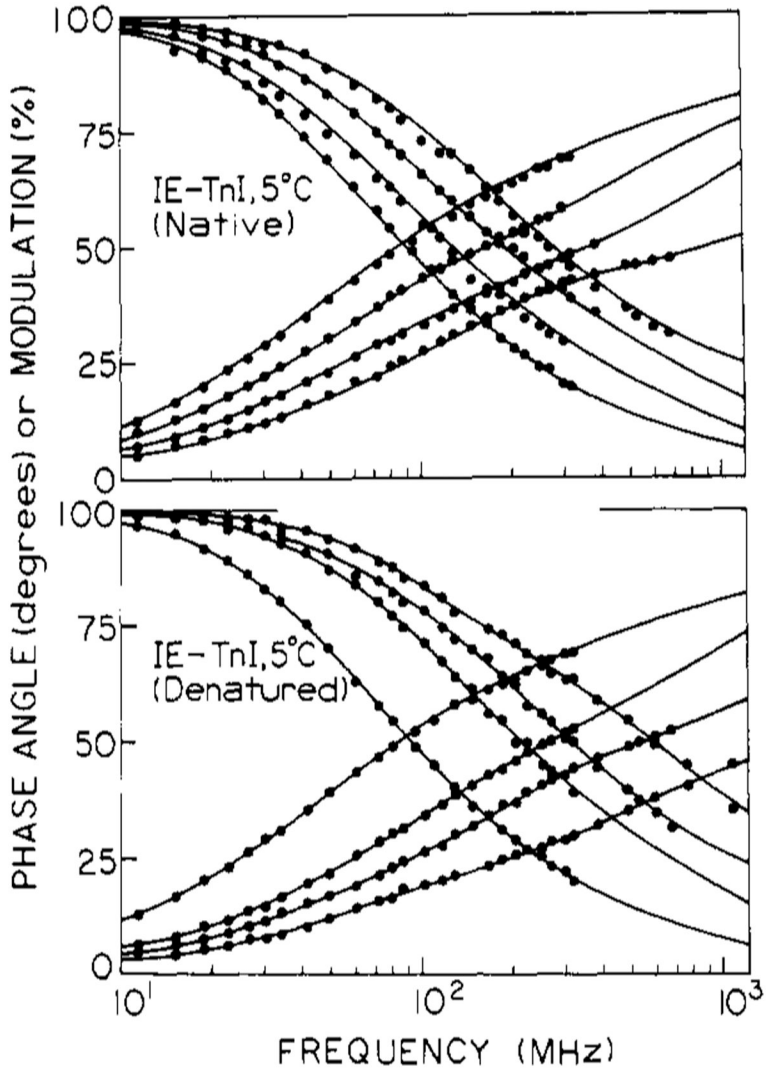

FIGURE 8:

Effects of guanidine hydrochloride on $\bar{r}$ and hw of the D–A distribution of TnI (●) and the TnI·TnC + Ca^{2+} complex (○). Gdn-HCl was added by using appropriate volumes of the Gdn-HCl-containing buffer (Materials and Methods).

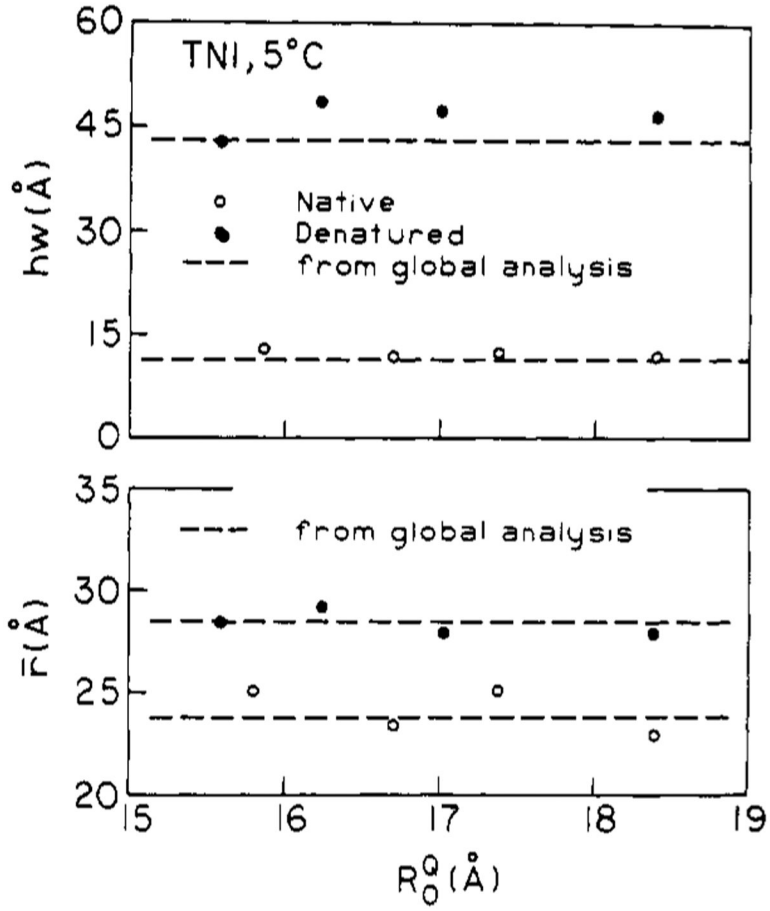

FIGURE 9:

Global distance distribution analysis for native (top) and denatured (bottom) IE-TnI at acrylamide concentrations of 0, 0.2, 0.4, and 0.8 M (top, left to right) and 0, 0.2, 0.4, and 0.65 M acrylamide (bottom, left to right). The R_0^Q values are summarized in Table IV. The solid lines are for global fits to the data at all acrylamide concentrations. For native TnI (top) $\bar{r}$ = 23.5 Å and hw = 10.1 Å. For denatured TnI (bottom) $\bar{r}$ = 28.7 Å and hw = 44.6 Å.

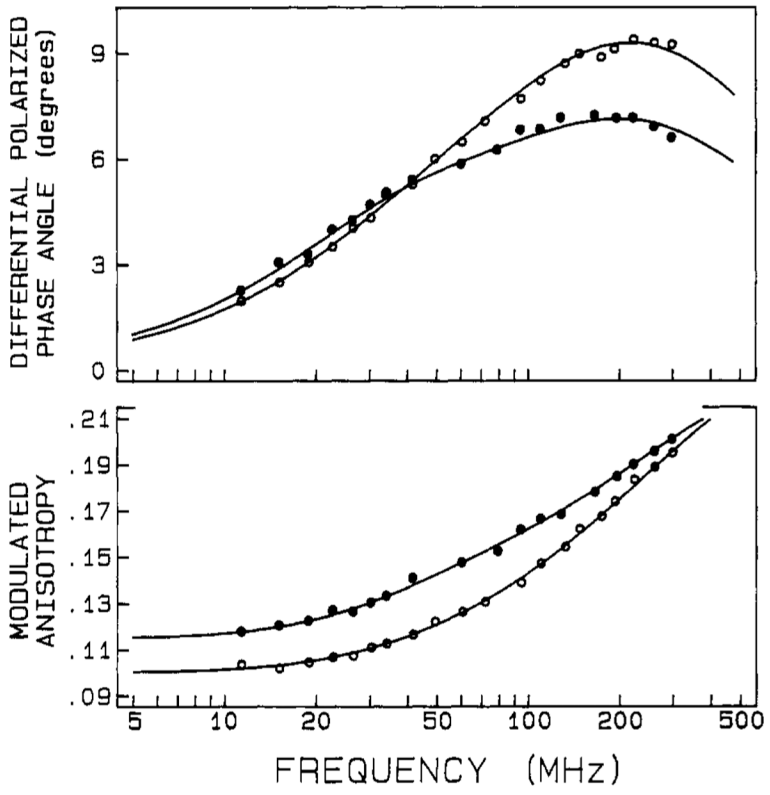

FIGURE 10:

Dependence of the distance distribution on R_0^Q for native and denatured IE-TnI. The data (○, ●) indicate the values recovered by analysis of each file individually, and the dashed lines are the result of simultaneous analysis of the data obtained at four acrylamide concentrations.

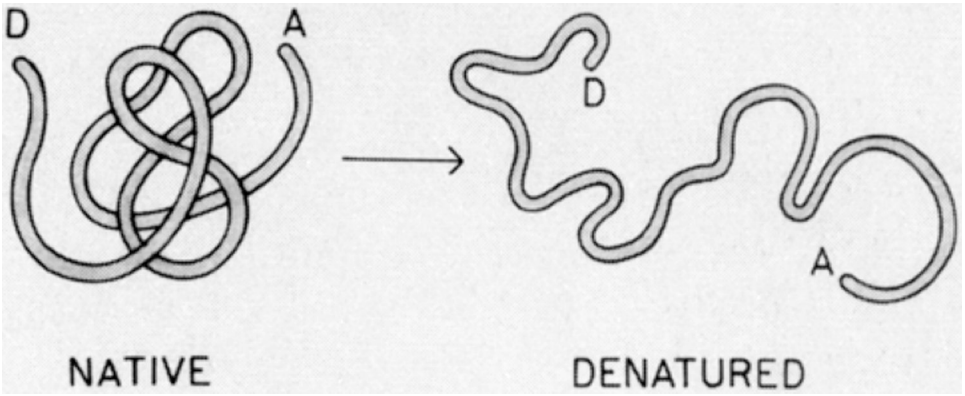

FIGURE 11:

Frequency-domain anisotropy data for native and denatured TnI. Data are shown for native (●) and denatured (○, 5 M Gdn-HCl) TnI. For native TnI, θ_1 = 0.66 ns, θ_2 = 8.89 ns, r_1 = 0.101, and r_2 = 0.139. For denatured TnI, θ_1, = 0.67 ns, θ_2 = 7.12 ns, r_1 = 0.144, and r_2 = 0.105.

Table I:

Analysis of Simulated Data for Donor–Acceptor Pairs

simulated values[a]		recovered values[b]		standard deviation of[c]		range of[d]		χ_R^2 for[e]	
$\bar{r}$ (Å)	hw (Å)	$\bar{r}$ (Å)	hw (Å)	$\bar{r}$ (Å)	hw (Å)	$\bar{r}$ (Å)	hw (Å)	single τ fit	distance fit
25	0.1	24.99	0.10	0.02	0.02	24.90–25.10	−2.39–2.39[g]	1.13	1.15
25	0.5	25.01	0.50	0.02	0.00	24.90–25.09	−2.57–2.57	1.03	1.06
25	1.0	25.02	1.12	0.04	0.43	24.92–25.12	−2.70–2.70	1.09	1.11
25	2.0	25.00	1.89	0.05	0.59	24.90–25.11	−2.87–3.08	1.16	1.17
25	4.0	25.01	4.04	0.06	0.46	24.89–25.15	3.05–4.84	1.30	1.13
25	5.0	24.98	4.69	0.05	0.36	24.82–25.16	3.88–5.61	1.58	1.18
25	8.0	25.05	8.15	0.08	0.37	24.88–25.20	7.40–8.85	5.64	1.11
25	10.0	25.02	9.99	0.05	0.17	24.86–25.16	9.28–10.65	11.62	1.16
25	25.0	24.96	25.22	0.23	0.91	24.53–25.27	23.44–27.56	66.36	1.14
25	50.0	24.91	49.79	1.93	5.78	21.42–29.20	42.38–60.72	52.66	1.14
15	5.0	15.01	4.97	0.03	0.06	14.94–15.09	4.79–5.15	69.48	1.13
15	50.0	14.60	50.54	3.2	5.03	9.45–18.47	44.22–58.65	104.20	1.13
25[f]	1.0	25.01	0.97	0.03	0.32	24.90–25.15	−2.83–2.83	445	1.16
25	5.0	25.0	4.75	0.12	1.08	24.81–25.22	2.69–5.95	451	1.13
25	50.0	25.05	48.93	2.68	4.19	20.38–27.94	40.04–63.00	638	1.45

[a] The simulated frequency-domain data included phase and modulation values at 22 frequencies, spaced approximately equally on a log scale from 10 to 320 MHz. The value of τ_D was taken as 3 ns, and R_0 was 20 Å. Random noise was added with $\delta\phi = 0.2°$ and $\delta m = 0.005$.

[b] The recovered values are the average of 10–13 simulations, each with the same parameters but different random error values.

[c] The values shown are the standard deviations of the $\bar{r}$ and hw values recovered from the separate simulations.

[d] The range shown is the average from the separate simulations, each calculated according to Johnson (1983).

[e] Average value of χ_R^2 for single decay time fits and the distance distribution fits.

[f] For all the following simulations $\tau_{D1} = 0.3$, $\tau_{D2} = 1.0$, and $\tau_3 = 3.0$, with $\alpha_{D1} = \alpha_{D2} = \alpha_{D3} = 0.333$.

[g] The negative values of hw are not important because this parameter appears only as its square (eq 12), and the distance-integrated probability is normalized (eq 18).

Table II:

Intensity Decays of Trp 158 in Troponin I

sample	τ_i (ns)	α_i	f_i	χ_R^2
TnI (D)[a]	3.10	1.0	1.0	528.3[b]
	0.93	0.51	0.17	
	4.64	0.49	0.83	5.4
	0.53	0.35	0.07	
	2.23	0.34	0.29	
	5.39	0.31	0.64	1.6
IE-TnI (D + A)	2.42	1.0	1.0	654.1
	0.71	0.53	0.18	
	3.80	0.47	0.82	5.8
	0.56	0.44	0.12	
	2.50	0.37	0.43	
	5.02	0.19	0.45	2.4
TnI·TnC + EGTA (D)	3.05	1.0	1.0	518.1
	0.86	0.50	0.16	
	4.47	0.50	0.84	8.7
	0.40	0.37	0.06	
	2.34	0.37	0.36	
	5.54	0.25	0.58	2.2
IE-TnI·TnC + EGTA (D + A)	2.40	1.0	1.0	756.6
	0.61	0.53	0.16	
	3.73	0.47	0.84	8.0
	0.43	0.45	0.10	
	2.41	0.37	0.45	
	5.11	0.18	0.45	1.8
TnI·TnC + Ca^{2+} (D)	3.00	1.0	1.0	553.8
	0.84	0.51	0.16	
	4.45	0.49	0.84	10.9
	0.57	0.42	0.10	
	3.26	0.49	0.63	
	7.65	0.09	0.27	2.7
IE-TnC·TnC + Ca^{2+} (D + A)	2.53	1.0	1.0	605.6
	0.69	0.52	0.16	
	3.82	0.48	0.84	8.7
	0.46	0.43	0.09	
	2.67	0.45	0.57	
	5.91	0.12	0.34	1.7
TnI·TnC + Mg^{2+} (D)	2.98	1.0	1.0	584.8
	0.74	0.48	0.14	
	4.31	0.52	0.86	8.7

sample	τ_i (ns)	α_i	f_i	χ_R^2
	0.37	0.37	0.06	
	2.16	0.34	0.34	
	5.19	0.29	0.64	2.1
IE-TnI·TnC + Mg^{2+} (D + A)	2.48	1.0	1.0	644.0
	0.59	0.52	0.15	
	3.67	0.48	0.85	10.2
	0.25	0.46	0.06	
	2.06	0.34	0.40	
	4.77	0.20	0.54	1.5
TnI–6 M Gdn-HCl (D)	2.72	1.0	1.0	362.8
	0.82	0.45	0.15	
	3.79	0.55	0.85	5.2
	0.64	0.37	0.10	
	3.02	0.53	0.66	
	6.07	0.10	0.24	2.6
IE-TnC + 5 M Gdn-HCl (D + A)	2.42	1.0	1.0	475.7
	0.65	0.49	0.15	
	3.47	0.51	0.85	5.7
	0.43	0.40	0.09	
	2.40	0.43	0.51	
	4.80	0.17	0.40	1.8

[a] D indicates unlabeled TnI and D + A indicates IE-labeled TnI.

[b] Calculated by using $\delta\phi = 0.2°$ and $\delta m = 0.005$.

Table III:

Distance Distribution between Trp 158 and Cys 133 in Troponin I

sample	R_0 (Å)[a]	n[b]	$\bar{r}$ (Å)	hw (Å)	χ_R^2
TnI	18.4	0	24.3	11.5	2.8
				⟨2⟩[c]	6.7
		1	23.3	11.9	2.8
		2	23.1	12.3	2.8
TnI·TnC + EGTA	19.2	0	26.3	19.7	3.0
				⟨2⟩	15.9
TnI·TnC + Ca^{2+}	19.4	0	27.4	11.5 (14.5)[d]	2.1
				⟨2⟩	3.1
TnI·TnC + Mg^{2+}	19.2	0	27.5	21.4	4.0
				⟨2⟩	12.4
TnI + 6 M Gdn-HCl	18.4	0	27.0	55.9	3.0
				⟨2⟩	14.8
		1	−77.7[e]	115.4	3.1
		2	−160.0	104.6	3.2

[a] From Wang (1979).

[b] As in r^n, eq 10.

[c] The broken brackets (⟨ ⟩) indicate the parameter was held fixed at the indicated value during the least-squares analysis.

[d] The value of 14.5 Å was found in a second separate experiment.

[e] The negative values of $\bar{r}$ do not represent negative distances but simply define the shape of $P(r)$ with $n = 1$ or 2.

Table IV:

Forster Distances for IE-TnI in the Presence of Acrylamide

	R_0^Q (Å)			R_0^Q (Å)	
[acrylamide]	**native**[a]	**denatured**[b]	**[acrylamide]**	**native**[a]	**denatured**[b]
0	18.40	18.40	0.65		15.56
0.2	17.38	17.02	0.80	15.84	
0.4	16.71	16.22			

[a] Calculated by using R_0 = 18.4 Å and K_D = 2.9 M^{-1}.

[b] Calculated by using R_0 = 18.4 Å and K_D = 4.35 M^{-1}.

Table V:

Anisotropy Decays of Trp 158 and IE-Cys 133 in Troponin I

sample	emitter[a]	θ_i (ns)	r_i	1θ	2θ	χ_R^2 d_i[b]
TnI	Trp	0.66	0.101			
		8.89	0.139	53.4	1.0	0.58
TnI·TnC	Trp	1.16	0.159			
		22.06	0.087	58.9	0.86	0.35
TnI·TnC + Ca^{2+}	Trp	1.41	0.162			
		19.78	0.081	34.2	0.72	0.33
TnI + 6 M Gdn-HCl	Trp	0.67	0.144			
		7.12	0.105	49.1	0.79	0.42
IE-TnI	IE	1.96	0.091			
		14.75	0.151	29.1	2.20	0.62
IE-TnF·TnC	IE	2.32	0.113			
		21.05	0.128	55.5	0.68	0.53
IE-TnI·TnC + Ca^{2+}	IE	3.16	0.120			
		21.57	0.131	43.1	1.45	0.52
IE-TnI + 5 M Gdn-HCl	IE	1.95	0.193			
		6.35	0.046	2.8	0.77	0.19

[a] Conditions were the same as listed in Table IV; excitation was at 295.5 nm for Trp and 360 nm for IE.

[b] Calculated from $r_i/\sum r_i$, according to eq 35.

Table VI:

Steady-State Anisotropies for Trp 158 and IE-Cys 133 in Troponin I

	anisotropies[a]		depolarization factor[b]	
sample	Trp 158	IE-Cys 133	$\langle d_D^x \rangle$	$\langle d_A^x \rangle$
TnI	0.117	0.099	0.793	0.914
TnI·TnC (EGTA)	0.115	0.100	0.737	0.600
TnI·TnC + Ca^{2+}	0.112	0.097	0.728	0.580
TnI·TnC + Mg^{2+}	0.111	0.096	0.724	0.759
TnI + 6 M Gdn-HCl	0.103	0.053	0.744	0.564

[a]For Trp 158 the excitation was at 295.5 nm, and the emission was observed at 340 nm. For these conditions the fundamental anisotropy (r_0) by NATA is 0.238. For IE-TnI (Cys 133) the excitation was at 360 nm/295.5 nm, and the emission was observed at 500 nm. For these conditions the fundamental anisotropies (r_0) are 0.25 and 0.175, respectively.

[b]Calculated by using $\langle d_I^x \rangle = (r_S/r_0)^{1/2}$, as described by Dale and Eisinger (1975). The value of r_S is the value of the steady-state anisotropy, approximately corrected for overall rotational diffusion, as described by eq 33-34. The values of τ were taken as 2.5 and 10 ns for Trp and IE, respectively, and the value of θ as taken as 9 ns for TnI and 20 ns for TnI·TnC.